Multiscale Eddy Simulation for Moist Atmospheric Convection: Preliminary Investigation

Samuel N. Stechmann[a,*]

[a]*Department of Mathematics, and Department of Atmospheric and Oceanic Sciences, University of Wisconsin–Madison, USA*

Abstract

A multiscale computational framework is designed for simulating atmospheric convection and clouds. In this multiscale framework, large eddy simulation (LES) is used to model the coarse scales of 100 m and larger, and a stochastic, one-dimensional turbulence (ODT) model is used to represent the fine scales of 100 m and smaller. Coupled and evolving together, these two components provide a multiscale eddy simulation (MES). Through its fine-scale turbulence and moist thermodynamics, MES allows coarse grid cells to be partially cloudy and to encompass cloud–clear air mixing on scales down to 1 m; in contrast, in typical LES such fine-scale processes are not represented or are parameterized using bulk deterministic closures. To illustrate MES and investigate its multiscale dynamics, a shallow cumulus cloud field is simulated. The fine-scale variability is seen to take a plausible form, with partially cloudy grid cells prominent near cloud edges and cloud top. From earlier theoretical work, this mixing of cloudy and clear air is believed to have an important impact on buoyancy. However, contrary to expectations based on earlier theoretical studies, the mean statistics of the bulk cloud field are essentially the same in MES and LES; possible reasons for this are discussed, including possible limitations in the present formulation of MES. One difference between LES and MES is seen in the coarse-scale turbulent kinetic energy, which appears to grow slowly in time due to incoherent stochastic fluctuations in the buoyancy. This and other considerations suggest the need for some type of spatial and/or temporal filtering to attenuate undersampling of the stochastic fine-scale processes.

Keywords:
large eddy simulation, one-dimensional turbulence, stochastic modeling, shallow cumulus clouds, atmospheric boundary layer

1. Introduction

Models of atmospheric dynamics must focus on a limited range of scales and physics, due to limited computational resources. For example, simulations of cloud systems of $O(100)$ *kilometers* must use grid spacings of $O(100)$ *meters* [1, 2, 3]. With such grid spacings, a great deal of subgrid-scale processes must be represented in some way. Subgrid-scale turbulence is typically represented via a large eddy simulation (LES) framework, and other key ingredients are thermodynamics and cloud microphysics involving subgrid-scale water substance: vapor, liquid droplets, phase changes, droplet collision/coalescence, etc. [4, 5, 6].

In models of subgrid-scale cloud processes, traditional approaches are computationally inexpensive but physically unsatisfying—if not inadequate—in several ways. First, as one example, a grid cell must be either entirely saturated or entirely unsaturated. It has long been realized that this is unrealistic for grid spacings of $O(100)$ m [7, 8]. While some interesting work has been proposed to mitigate this issue [9, 10], no method has yet been generally accepted. Second, as another example, subgrid-scale turbulence typically interacts very weakly—if at all—with subgrid-scale thermodynamics and cloud microphysics. A great deal of work has examined the effect of turbulence on droplet

*Corresponding author
Email address: stechmann@wisc.edu (Samuel N. Stechmann)
URL: http://www.math.wisc.edu/~stechmann/ (Samuel N. Stechmann)

collisions [11, 12, 13] and the thermodynamic impact of turbulent mixing of cloudy and clear air [14, 15, 16, 17]; and these effects are being incorporated into some interesting new subgrid-scale parameterizations [18, 19, 20]. In short, as illustrated by these examples, the intermingling of different processes on different scales has received increasing attention, and it is becoming apparent that new theoretical and computational tools are needed [21, 22].

The main purpose of this paper is to investigate a multiscale modeling approach to cloud dynamics. Instead of the typical "grid scales" and "subgrid-scales", the multiscale framework involves a "coarse-scale" grid, a "fine-scale" grid, and two models: on the coarse scales of >100 m is an LES model, and on the fine scales of <100 m is a stochastic, one-dimensional turbulence (ODT) model [23, 24, 25, 26, 27]. Coupled and evolving together, these two components form a multiscale eddy simulation (MES).

A key goal of the multiscale approach is to include more realistic fine-scale behavior—in particular, to allow fine-scale regions of cloudy and cloud-free air to mix turbulently. Previous work [28, 29, 30] has shown the importance of the finite time scales of such mixing—as opposed to slow mixing or instantaneous mixing scenarios—and some studies [31, 15, 16, 17] investigated such mixing with a predecessor of the ODT model. If the fine-scale mixing and its thermodynamic impact are represented more realistically, it is expected that, in turn, the coarse-scale behavior will be more realistic as well.

Multiscale modeling has been a successful approach in many related scientific areas. Problems such as turbulent combustion involve multiscale phenomena with chemical reactions interacting with turbulent fluid dynamics [32], which are similar to the issues of phase changes and droplets in cloud dynamics. In fact, LES and ODT have been used in both combustion and atmospheric science [33, 26, 34] and models that combine LES and ODT dynamics have been proposed previously for combustion [35] and for general turbulent flows [36, 37]. The multiscale framework of the present paper is different from these previous approaches and is similar in spirit to the "superparameterization" approach that has been used for much larger scales of atmospheric dynamics [38, 39, 40, 41, 42]. On the fine scales, a 1D or 2D reduced-dimensional model is used, and it uses periodic boundary conditions within each coarse cell. This configuration simplifies the multiscale coupling and is well-suited for massively parallel computations in an "embarrassingly parallel" setup. It may also be a useful framework for other scientific areas with similar challenges, such as turbulent combustion, ocean dynamics [43, 44], or bubbles in the ocean [45].

Besides multiscale computational models, multiscale asymptotic models have also been useful for elucidating interactions between different scales. In atmospheric science, many such models have been investigated for elucidating interactions between clouds, their environment, and the larger-scale circulation [46, 47]. In particular, those most related to the present investigation are [48] and [49], which investigate boundary layer clouds—stratocumulus and shallow cumulus clouds, respectively.

Among the various cloud regimes that could be modeled with the multiscale framework, the particular focus of the present paper is shallow cumulus clouds. These clouds are "shallow" as opposed to "deep" in the sense that they extend vertically only a few kilometers above the Earth's surface [50]. Moreover, they are somewhat simple in the sense that they do not involve ice and they often do not rain; nevertheless, they still involve the challenges of turbulent mixing and vapor–liquid phase changes over a large range of scales, which makes them well-suited as a test case for MES.

From a broader perspective, the multiscale framework is ultimately aimed at enhancing our understanding of clouds and their role in the climate system [51, 52]. In this capacity, clouds play an important role in both the Earth's radiation budget and hydrological cycle. A remarkable range of scales is involved: microscale aerosols and liquid droplets affect macroscale cloud properties such as size, lifetime, propensity to rain, and ability to scatter or absorb electromagnetic radiation [53, 54, 55, 56, 22]. Further complicating matters, all of these microscale and macroscale processes are intricately linked with turbulent mixing. While this complicated setting is the ultimate motivation, here we use a simplified setup that neglects intricate radiation, aerosol, and precipitation effects and instead focuses on the pervasive turbulent mixing that make these effects so perplexing. Furthermore, the turbulent mixing of ODT is used here for its effect on buoyancy alone, and not for use as a stochastic model of fine-scale turbulent fluxes. Instead, a Smagorinsky closure is retained for modeling the effect of "subgrid-scale" turbulent fluxes on the coarse-scale flow field. In principle, ODT could be used for this purpose in place of the Smagorinsky model, but a preliminary investigation presented formidable challenges in this direction, and we leave this as an interesting direction to pursue further in the near future. In short, the ODT model will be used here to investigate only the impact of fine-scale mixing on the buoyancy in non-precipitating clouds.

The paper is organized as follows. In section 2, the multiscale model is described, including both the LES and

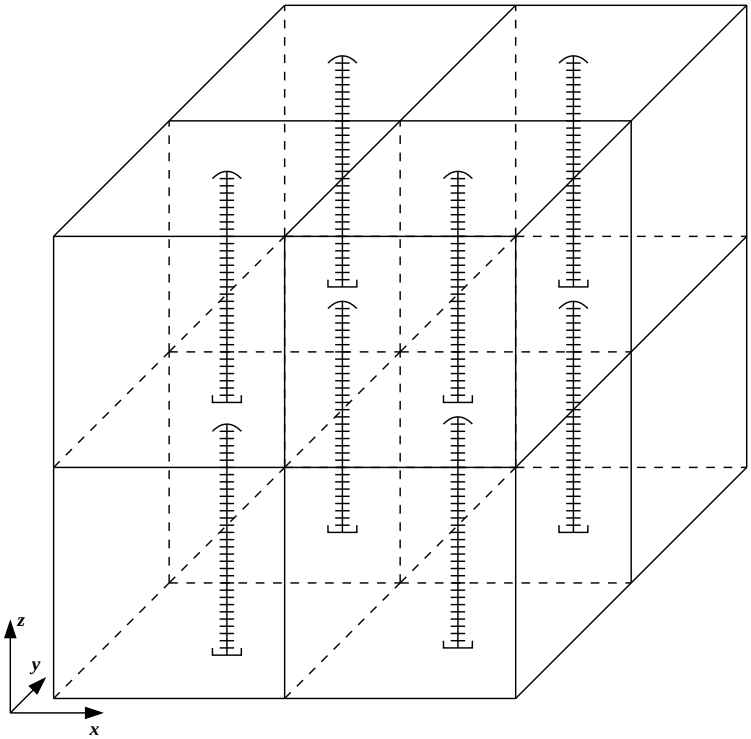

Figure 1: Eight coarse grid cells of MES, each with an embedded ODT line.

ODT components and their coupling to form the MES. In section 3, a one-way coupled version of MES is examined in which the coarse LES model affects the fine ODT model but not vice versa; this configuration provides a simplified view of the fine-scale dynamics, and it allows a comparison of coarse and fine scales on a cell-by-cell basis. Then, in section 4, the full MES model is investigated where two-way coupling is allowed between coarse and fine scales; and MES statistics are compared with LES. Finally, in section 5, conclusions are summarized and future directions are discussed.

2. Model description

The multiscale framework involves "coarse scales" and "fine scales", along with both a coarse-scale grid and a fine-scale grid, as depicted in Figure 1. Associated with each of these grids is a different model dynamics: LES dynamics on the coarse grid, and ODT dynamics on the fine grid. The LES grid is a regular 3D Cartesian grid, and embedded within each coarse cell is a 1D line segment for ODT dynamics. For the scales of interest here, the coarse cell width is chosen to be $\Delta X = 100$ m; correspondingly, each ODT line is 100 m in length with a fine cell width of $\Delta x = 1$ m. Note that, while ODT involves equations on a 1D line, it is designed to model the properties of 3D turbulence [23, 24, 25, 26]. Below, the coarse LES model and fine ODT model are described individually in sections 2.1 and 2.2, respectively, and then the MES coupling is presented in section 2.3.

2.1. Coarse-scale LES model

The LES model here is the UCLA LES model [57], which evolves the Ogura–Phillips anelastic equations for the velocity $\bar{\mathbf{u}} = (\bar{u}, \bar{v}, \bar{w})$, the liquid-water potential temperature $\bar{\theta}_l$, and the total water mixing ratio $\bar{q}_t$:

$$\frac{\partial \bar{u}_i}{\partial T} = -\bar{u}_j \frac{\partial \bar{u}_i}{\partial X_j} - c_p \Theta_0 \frac{\partial \bar{\pi}}{\partial X_i} + g \frac{\bar{\theta}_v''}{\theta_0} \delta_{i3} + \frac{1}{\rho_0} \frac{\partial (\rho_0 \tau_{ij})}{\partial X_j} \qquad \text{for } i = 1, 2, 3 \tag{1}$$

$$\frac{\partial \bar{\theta}_l}{\partial T} = -\bar{u}_j \frac{\partial \bar{\theta}_l}{\partial X_j} + \frac{1}{\rho_0} \frac{\partial (\rho_0 \gamma_{\theta_l j})}{\partial X_j} \tag{2}$$

$$\frac{\partial \bar{q}_t}{\partial T} = -\bar{u}_j \frac{\partial \bar{q}_t}{\partial X_j} + \frac{1}{\rho_0} \frac{\partial (\rho_0 \gamma_{q_t j})}{\partial X_j} \tag{3}$$

along with the anelastic continuity equation

$$\frac{\partial (\rho_0 \bar{u}_i)}{\partial X_i} = 0 \tag{4}$$

The ambient density $\rho_0(z)$ is fixed, and subgrid-scale fluxes τ_{ij}, $\gamma_{\theta_l j}$, and $\gamma_{q_t j}$ are closed using the Smagorinsky–Lilly model. The Einstein summation convention is used in (1)–(4) with the alternative notations $\bar{\mathbf{u}} = (\bar{u}_1, \bar{u}_2, \bar{u}_3)$ and $\mathbf{X} = (X_1, X_2, X_3)$ for brevity. The overbar denotes that the LES variables are defined on the coarse grid, and capital letters T and $\mathbf{X} = (X, Y, Z)$ denote the coarse time and spatial coordinates.

The buoyancy in (1) is defined in terms of $\bar{\theta}_v''$, where $\bar{\theta}_v$ is the virtual potential temperature defined as

$$\bar{\theta}_v = \bar{\theta} \left[1 + \left(\frac{R_v}{R_d} - 1 \right) \bar{q}_v - \bar{q}_l \right], \qquad \bar{q}_l = \max \Big(0 \ , \ \bar{q}_t - q_{vs}(\bar{T}, \bar{p}) \Big) \tag{5}$$

where $\bar{\theta}$, $\bar{q}_v$, $\bar{q}_l$, and $\bar{T}$ are recovered diagnostically from the two thermodynamic state variables, $\bar{\theta}_l$ and $\bar{q}_t$. The double prime on $\bar{\theta}_v''$ denotes the deviation from the horizontal average over the computational domain: $\bar{f}'' = \bar{f} - \iint \bar{f} \, dX \, dY$. In (5), also notice that the liquid water $\bar{q}_l$ is given diagnostically as the excess water content above the saturation value, $q_{vs}(\bar{T}, \bar{p})$. In this study, a simple case of moist convection is considered where precipitation is neglected and where only the bulk liquid water content $\bar{q}_l$ is modeled, not any details of the particular radii of the droplets.

The LES description in this subsection is for its use in isolation as an LES model, not as coupled with a fine-scale model; modifications to the LES model are needed for coupling it with a fine-scale model and are described later in subsection 2.3.

Notice that (5) defines thermodynamic relationships between coarse-scale variables such as $\bar{q}_t$ and $\bar{q}_l$, which are defined using a coarse grid spacing of $\Delta X = 100$ m. Such relationships ignore any fluctuations on smaller scales and treat each coarse cell as either entirely saturated or entirely unsaturated. In contrast, as described next, using a fine-scale model will allow thermodynamic relationships to be defined using the fine grid spacing of $\Delta X = 1$ m.

2.2. Fine-scale ODT model

ODT dynamics involves two components: (i) "eddy events", whose times, locations, and sizes are *stochastic*, and (ii) diffusion during the time periods between eddy events [23, 24, 25, 26]. These two ingredients reproduce the statistics of 3D turbulence, since the eddy events act to increase gradients and transfer energy to smaller scales, at which point the diffusion is most effective.

The diffusion is implemented along the ODT line as

$$\frac{\partial \theta_l'}{\partial t} = \nu \frac{\partial^2 \theta_l'}{\partial z^2}, \qquad \frac{\partial q_t'}{\partial t} = \nu \frac{\partial^2 q_t'}{\partial z^2}, \qquad \frac{\partial u'}{\partial t} = \nu \frac{\partial^2 u'}{\partial z^2}, \qquad \frac{\partial v'}{\partial t} = \nu \frac{\partial^2 v'}{\partial z^2}, \qquad \frac{\partial w'}{\partial t} = \nu \frac{\partial^2 w'}{\partial z^2} \tag{6}$$

For simplicity here, the eddy diffusion coefficient ν is taken to be constant, and the same value is used for the viscosity and diffusion for all variables (see the end of this subsection for a discussion of other options). As shown in (6), primes will be used to denote ODT fluctuations, which have mean zero:

$$\int s'(z) \, dz = 0, \tag{7}$$

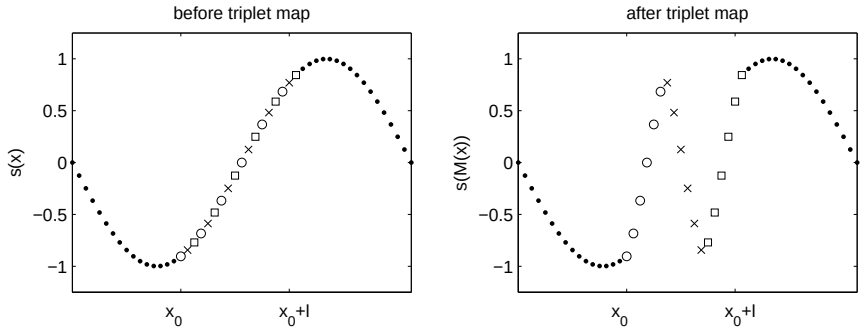

Figure 2: Triplet map illustration for the case of discrete grid points.

where s could be any of θ_l, q_t, u, v, w here. Also notice that lowercase z is used as the fine-scale coordinate, as opposed to the coarse-scale coordinates X, Y, Z; and the orientation of the ODT line is in the vertical z direction, for the purposes of this initial description, as shown in Figure 1. However, other orientations of the ODT line are also investigated and are described at the end of this subsection.

The stochastic eddy events are now described in two parts: first, the "eddy" itself is defined; and second, the stochastic *selection* of eddies is described in terms of the distribution of their times, locations, and sizes.

An ODT "eddy" is defined by rearranging the values of the model variables:

$$\theta_l'(z) \to \theta_l'(M(z)) \tag{8}$$
$$q_t'(z) \to q_t'(M(z)) \tag{9}$$
$$u'(z) \to u'(M(z)) + c_u K(z) \tag{10}$$
$$v'(z) \to v'(M(z)) + c_v K(z) \tag{11}$$
$$w'(z) \to w'(M(z)) + c_w K(z) \tag{12}$$

The rearrangment map $M(z)$ must have several properties to be suitable for incompressible turbulent flows; for instance, it must be measure-preserving in order to guarantee an analogue of incompressiblity. The choice that has been adopted for ODT is the triplet map, which is defined as

$$M(z) = z_0 + \begin{cases} 3(z-z_0) & \text{if} \quad z_0 \le z \le z_0 + \frac{1}{3}l \quad \text{(copy 1)} \\ 2l - 3(z-z_0) & \text{if} \quad z_0 + \frac{1}{3}l \le z \le z_0 + \frac{2}{3}l \quad \text{(copy 2, reversed)} \\ 3(z-z_0) - 2l & \text{if} \quad z_0 + \frac{2}{3}l \le z \le z_0 + l \quad \text{(copy 3)} \\ z - z_0 & \text{otherwise} \end{cases} \tag{13}$$

This map takes an interval $[z_0, z_0 + l]$ and replaces it by three shrunken versions of itself. The continuous mapping $M(z)$ is implemented on a discrete grid as shown in Figure 2.

In addition to rearrangement by the triplet map $M(z)$, the velocity components in (8)–(12) are altered by $K(z)$ terms. These additive terms represent energy redistributions. While they redistribute energy, they do not alter the total momentum due to the form of

$$K(z) = z - M(z) \tag{14}$$

which has an integral of zero. Also notice that $K(z)$ is only nonzero within the eddy interval $[z_0, z_0 + l]$, which is consistent with its use as an eddy-induced effect. As an example, if an eddy causes a change to the potential energy via $\theta_l'(z) \to \theta_l'(M(z))$ or $q_t'(z) \to q_t'(M(z))$, then the $c_i\, K(z)$ terms provide compensating changes to the kinetic energy, in order to conserve total energy. To meet this constraint of total energy conservation, the coefficients c_u, c_v, c_w for the energy redistribution are defined as

$$c_s = \frac{27}{4l}\left[-s_K \pm \sqrt{\frac{1}{3}\left(u_K^2 + v_K^2 + w_K^2 + \frac{8}{27}\frac{\theta_{v,K}}{\theta_0} g l\right)}\right] \tag{15}$$

where

$$s_K \equiv \frac{1}{l^2}\int s'(M(z))\,K(z)\,dz = \frac{4}{9l^2}\int_{z_0}^{z_0+l} s'(z)[l-2(z-z_0)]\,dz \tag{16}$$

See [26] for a derivation. Notice that adding a constant to $s(z)$ does not affect the value of s_K nor c_s; this fact will resurface below when considering eddy selection. With this definition of c_u, c_v, and c_w, the "eddy" in (8)–(12) is described completely.

To summarize, "eddies" are rearrangments by a measure-preserving map $M(z)$. They increase gradients and transfer energy to smaller scales, and at the same time they conserve momentum, water, entropy, and energy. Nevertheless, while total energy is conserved, energy is redistributed between kinetic and potential contributions, and energy is redistributed among velocity components; these redistributions are encoded in the $K(z)$ terms in (8)–(12).

With ODT "eddies" defined above, the next key ingredient is the stochastic *selection* of the eddies. This involves selection of the time, the location z_0, and the length l of an eddy. The distribution of these eddy properties is defined as $\lambda(z_0, l; t)\,dz_0\,dl\,dt$, where the density λ has units of $\mathrm{m}^{-2}\ \mathrm{s}^{-1}$ and is defined as

$$\lambda(z_0, l; t) = \frac{C}{l^3}\sqrt{u_K^2 + v_K^2 + w_K^2 + \frac{8}{27}\frac{\theta_{v,K}}{\theta_0}gl} \tag{17}$$

where C is a dimensionless free parameter. The quantities $u_K, v_K, w_K, \theta_{v,K}$ are defined in (16) and are measures of the velocity fluctuations and the potential energy change, respectively. Hence the expression inside the square root is a scaled form of the net available energy, and (17) is consistent with mixing-length phenomenology of turbulence [26].

A key aspect of the eddy-rate distribution in (17) is that it depends on the instantaneous state of the system: $u'(z,t), v'(z,t), w'(z,t), \theta_l'(z,t), q_t'(z,t)$. Consequently, new eddy events depend on previous eddy events—as would be the case for deterministic turbulence—and the stochastic eddy process inherently involves spatiotemporal correlations.

For the thermodynamic portion of (17), the ODT anomalies θ_l' and q_t' must be augmented by base state values $\bar{\theta}_l$ and $\bar{q}_t$ to define a true thermodynamic state with $\theta_l = \bar{\theta}_l + \theta_l'$ and $q_t = \bar{q}_t + q_t'$. From these two state variables, all other thermodynamic quantities can be obtained [5, 50]. The virtual potential temperature $\theta_v(z,t)$ can then be computed as

$$\theta_v = \theta\left[1 + \left(\frac{R_v}{R_d} - 1\right)q_v - q_l\right], \qquad q_l = \max(\,0\,,\ q_t - q_{vs}(T,p)\,) \tag{18}$$

In the multiscale framework that is the topic of this paper, the natural choice for $\bar{\theta}_l$ and $\bar{q}_t$ will be the coarse LES values, as described in section 2.3.

In principle, orienting the ODT line in the vertical z direction is convenient yet somewhat arbitrary. To explore a range of alternatives, orientations along the x and y axes will also be considered, in which case the ODT formulation follows [24]. For the diffusion, (6) is simply replaced by $\partial u'/\partial t = \nu\partial^2 u'/\partial x^2$, etc. or by $\partial u'/\partial t = \nu\partial^2 u'/\partial y^2$, etc. For the eddies, the eddy-rate distribution $\lambda(z_0, l; t)$ from (17) is replaced by

$$\lambda(x_0, l; t) = \frac{C}{l^3}\sqrt{u_K^2 + v_K^2 + w_K^2 - \frac{Z_{pen}\nu^2}{l^2}} \tag{19}$$

or similarly for $\lambda(y_0, l; t)$. Notice that (19) does not include a potential energy contribution for an x- or y-axis orientation of an ODT line; instead, it includes a "viscous penalty" term $Z_{pen}\nu^2/l^2$, where the free parameter Z_{pen} determines a critical Reynolds number for eddy turnover. Corresponding to this different eddy-rate distribution (19), the coefficients for energy redistribution take the values

$$c_s = \frac{27}{4l}\left[-s_K \pm \sqrt{\frac{1}{3}\left(u_K^2 + v_K^2 + w_K^2\right)}\ \right] \tag{20}$$

This definition does not involve redistribution of potential energy, as is appropriate for x- or y-axis orientations.

Only three free parameters entered into the ODT description above: ν, C, and Z_{pen}, from (6), (17), and (19), respectively. The parameter ν is an eddy diffusivity or viscosity rather than a molecular diffusivity or viscosity, since the fine grid spacing $\Delta x = 1$ m is too large to resolve molecular-transport properties. Here, for simplicity, ν is taken to

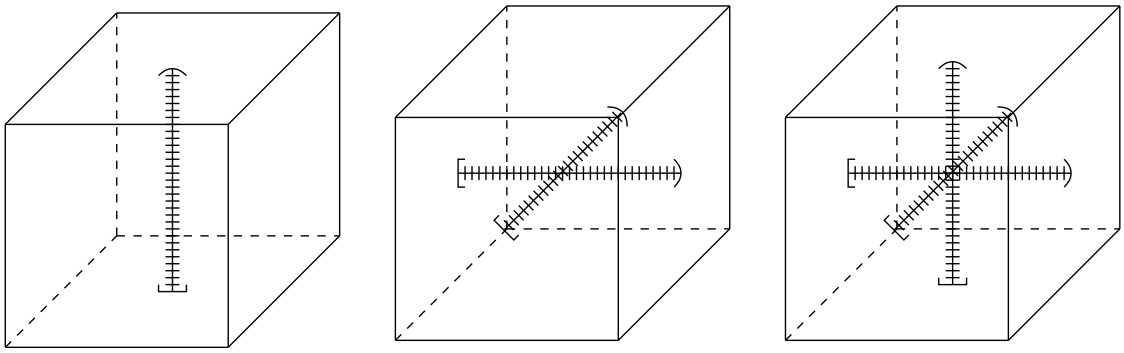

Figure 3: Options for including different ODT lines within each coarse cell. The ODT lines within a cell do not interact directly; they interact indirectly via the coarse dynamics.

be the constant $\nu = 0.02\ \mathrm{m}^2\ \mathrm{s}^{-1}$. In a sense, then, the ODT model provides a bridge between the LES-resolved scales and smaller scales that are farther down inside the turbulent cascade; and the eddy viscosity ν is used to model those scales below the ODT grid scale used here. Besides this simple choice of treating ν as a constant eddy viscosity, many other choices for modeling ν are possible: it could be a true molecular viscosity if the ODT grid spacing were small enough (roughly 1 mm for the present application), at considerable computational expense; it could be modeled by inheriting the LES scheme for unresolved turbulent transport (Smagorinsky for the present application) and applying this scheme on the ODT fine grid scale; or it could be modeled by an ensemble-mean limit of ODT dynamics, as is done in [36]; see [26] for more discussion of these options. The parameter C is a scaling factor for the eddy event rate and hence for the turbulence intensity. In broad agreement with previous ODT studies, the value $C = 10$ is used here. Finally, the parameter Z_{pen} is a "viscous penalty" that controls the critical Reynolds number for eddy turnover, and here its value is taken to be $Z_{pen} = 100$. These parameter choices and other configuration choices are influenced by—and benefited from—the many previous studies of the ODT model [23, 24, 25, 26].

To summarize, ODT involves stochastic "eddies" that are physically based on the mixing-length phenomenology of turbulence and are spatiotemporally correlated with previous eddy events. Consequently, the model includes intermittent fluctuations that are not just inherently statistical but are actually a physically based representation of turbulent intermittency. These attributes suggest the use of ODT as the fine-scale model in a multiscale framework.

2.3. MES model: coupling the coarse and fine scale models

The MES model is obtained by coupling the LES and ODT models. This coupling is nontrivial and is described in detail below. First the influence of the LES model on ODT is described, and then the influence of ODT on the LES model is described.

In brief, the coarse LES variables provide a slowly varying background environment for the fine-scale ODT dynamics, and averages of the ODT variables feed back on the LES dynamics. This coupling is carried out on a coarse-grid-cell by coarse-grid-cell basis, as illustrated schematically in Figure 1. The ODT line in one coarse cell does not *directly* interact with the ODT lines in other coarse cells. Instead, each ODT line is endowed with periodic boundary conditions within a single coarse cell, and different ODT lines interact *indirectly* through the coarse LES interactions. Such a multiscale framework is in the spirit of the "superparameterization" technique that has been used on much larger scales of atmospheric modeling [38, 39, 40, 41, 42]. In a similar spirit, ODT lines do not directly interact even for the configurations in Figure 3 with multiple ODT lines within each coarse cell. Consequently, the MES model is well-suited for massively parallel computations in an "embarrassingly parallel" setup.

2.3.1. LES influence on ODT

Coarse LES variables affect the fine ODT variables in three ways: (i) in the definition of thermodynamic state variables on the fine grid, (ii) in the eddy-rate distribution, and (iii) in the eddy implementation.

First, as mentioned near (18), the ODT anomalies θ_l' and q_t' must be augmented by base state values $\bar{\theta}_l$ and $\bar{q}_t$ in order to define a true thermodynamic state with

$$\theta_l = \bar{\theta}_l + \theta_l' \qquad \text{and} \qquad q_t = \bar{q}_t + q_t'. \tag{21}$$

The natural choice for MES is to use the coarse LES values for $\bar{\theta}_l$ and $\bar{q}_t$ and to compute thermodynamic relationships as in (18):

$$\theta_v = \theta\left[1 + \left(\frac{R_v}{R_d} - 1\right)q_v - q_l\right] \qquad q_l = \max\left(\,0\,,\; q_t - q_{vs}(T,p)\,\right), \tag{22}$$

where θ, q_l, etc. are thermodynamic variables computed at each fine grid cell.

Second, LES coarse gradients provide a background state in which the ODT eddies evolve. In particular, the ODT eddy-rate distribution (17) now uses a modified version of the measure (16) of eddy fluctuations:

$$s_K \equiv \frac{4}{9l^2}\int_{z_0}^{z_0+l}\left[s(z) + z\frac{\partial \bar{s}}{\partial Z}\right][l - 2(z - z_0)]\,dz \tag{23}$$

which now includes the linear-in-z contribution due to the coarse background derivative, $\partial\bar{s}/\partial Z$. [In the definition (23), notice that adding a constant to $s(z)$ does not affect the value of s_K; consequently, it is irrelevant whether the total $s(z)$ or ODT contribution $s'(z)$ is used to compute s_K.] The coarse gradient contribution in (23) can be expected to play an important role wherever there are, for instance, large shears $\partial\bar{u}/\partial Z$, strains $\partial\bar{w}/\partial Z$, or thermodynamic derivatives $\partial\bar{\theta}_v/\partial Z$.

Third, the LES coarse gradients affect the shape of ODT eddy anomalies. In particular, a coarse gradient can create a couplet of a new positive positive anomaly adjacent to a new negative anomaly. An illustration of this is shown in Figure 4, where the ODT anomaly is initially zero, but a couplet anomaly is created after an eddy event in the presence of a coarse gradient. For cloud dynamics, it is this important mechanism that can create a partially cloudy cell from a cell that is initially uniform in its thermodynamic state. In equation form, this mechanism can be described in the following way. For eddies in MES, the triplet map is applied not only to the ODT fluctuation $s'(z)$ but also to a linear component $z(\partial\bar{s}/\partial Z)$ which inherits its slope from the coarse derivative; i.e., (8)–(12) are replaced by

$$\theta_l'(z) + z\frac{\partial\bar{\theta}_l}{\partial Z} \to \theta_l'(M(z)) + M(z)\frac{\partial\bar{\theta}_l}{\partial Z} \tag{24}$$

$$q_t'(z) + z\frac{\partial\bar{q}_t}{\partial Z} \to q_t'(M(z)) + M(z)\frac{\partial\bar{q}_t}{\partial Z} \tag{25}$$

$$u'(z) + z\frac{\partial\bar{u}}{\partial Z} \to u'(M(z)) + M(z)\frac{\partial\bar{u}}{\partial Z} + c_u K(z) \tag{26}$$

$$v'(z) + z\frac{\partial\bar{v}}{\partial Z} \to v'(M(z)) + M(z)\frac{\partial\bar{v}}{\partial Z} + c_v K(z) \tag{27}$$

$$w'(z) + z\frac{\partial\bar{w}}{\partial Z} \to w'(M(z)) + M(z)\frac{\partial\bar{w}}{\partial Z} + c_w K(z) \tag{28}$$

where dependence on X, Y, Z, T has been suppressed in notation above. Also note that the definition (15) of c_u, c_v, and c_w must now use the modified form (23) of s_K, which accounts for the coarse derivative, instead of the original in (16). Since (24)–(28) include both the ODT fluctuation $s'(z)$ and also the coarse gradient term $z(\partial\bar{s}/\partial Z)$, they do not explicitly show the couplet anomaly. To isolate the couplet anomaly more clearly, the coarse derivatives $z(\partial\bar{s}/\partial Z)$ can

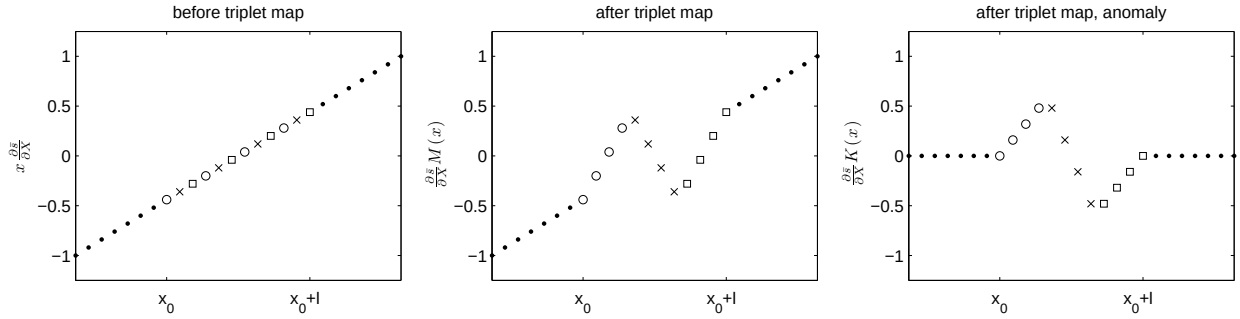

Figure 4: Triplet map illustration in the presence of a coarse gradient. Shows both continuous and discrete versions. Left: a fine-scale state $x(\partial\bar{s}/\partial X)$ in the presence of coarse derivative with zero fine-scale anomaly. Middle: rearrangement $M(x)(\partial\bar{s}/\partial X)$ of left panel using the triplet map. Right: the anomaly created by the triplet map in the presence of the coarse derivative. The anomaly is computed by subtracting the left panel from the middle panel: $(\partial\bar{s}/\partial X)M(x) - (\partial\bar{s}/\partial X)x = -(\partial\bar{s}/\partial X)K(x)$

be subtracted from both sides of (24)–(28), to give

$$\theta_l'(z) \to \theta_l'(M(z)) - \frac{\partial\bar{\theta}_l}{\partial Z}K(z) \tag{29}$$

$$q_t'(z) \to q_t'(M(z)) - \frac{\partial\bar{q}_t}{\partial Z}K(z) \tag{30}$$

$$u'(z) \to u'(M(z)) - \frac{\partial\bar{u}_t}{\partial Z}K(z) + c_u K(z) \tag{31}$$

$$v'(z) \to v'(M(z)) - \frac{\partial\bar{v}_t}{\partial Z}K(z) + c_v K(z) \tag{32}$$

$$w'(z) \to w'(M(z)) - \frac{\partial\bar{w}}{\partial Z}K(z) + c_w K(z) \tag{33}$$

In this form, one can see the important difference from the stand-alone ODT version (8)–(12): a couplet anomaly $(\partial\bar{s}/\partial Z)K(z)$ is created due to the coarse derivative $\partial\bar{s}/\partial Z$. The function $K(z)$ was defined in (14) and is illustrated in the right panel of Figure 4. This is an additional anomaly that can be created even if the ODT variable $s'(z)$ was initially zero before implementing the triplet map, as in the case in Figure 4. To some extent, this represents the process of engulfing a portion of cloudy air during an entrainment event. Through this key mechanism, fine-scale fluctuations are enhanced in regions of large coarse-scale derivatives, such as cloud edges and the rising cloud top.

Note that the mechanism in (29)–(33) and Figure 4 is present in ODT but absent from the ODT model's predecessor, the linear eddy model (LEM) [31]. With LEM, given two fluids with different properties, it is necessary to first place (or "splice") them next to each other, after which LEM can proceed to mix the two fluids. This type of "splicing" was an imporant aspect of an early use of LEM as a subgrid-scale model for LES [58] and a model for entrainment and mixing in clouds [15, 16]. With ODT instead of LEM, such "splicing" appears to be unnecessary because the mechanism in Figure 4 appears to create neighboring regions with different fluid properties as a natural part of the ODT algorithm. Furthermore, the eddy event in Figure 4 has a flux associated with it (see section III.E. of [59] for an explicit definition), and the flux is related to the coarse derivative $\partial\bar{s}/\partial Z$). This flux represents a turbulent transport that is induced by the coarse-scale flow, and, as such, it could be used as a model for fine-scale turbulent fluxes in place of a traditional model such as the Smagorinsky scheme. However, in a preliminary investigation of using ODT fluxes in place of the Smagorinsky scheme, we came across formidable challenges, and so we leave this as an interesting direction to pursue further in the near future. It would also be interesting to consider the use of a "splicing" method or a related method in the future. At the present time, however, we retain the Smagorinsky scheme, and we explore the fine-scale transport mechanism of Figure 4 that is naturally built into ODT.

In short, coarse gradients can create fine-scale anomalies, and, particularly near cloud edges and cloud top, they can create fine-scale regions of cloudy air surrounded by cloud-free air. As earlier theoretical work has shown, the subsequent mixing of the cloudy and clear air can have an important impact on the buoyancy [14, 15, 16]. These effects will be explored below in the context of MES.

2.3.2. ODT influence on LES

The fine-scale ODT model will affect the coarse-scale LES model in only one aspect here: the buoyancy. As shown in (1), the buoyancy is defined in terms of the virtual potential temperature $\bar{\theta}_v$, which in a multiscale framework should be an average over the fine scales:

$$\bar{\theta}_v = \overline{\theta \left[1 + \left(\frac{R_v}{R_d} - 1 \right) q_v - q_l \right]}, \qquad \bar{q}_l = \overline{\max (0 \, , \; q_t - q_{vs}(T, p))}, \tag{34}$$

Notice that (34) is different from the traditional LES definition of $\bar{\theta}_v$ as in (5); whereas (5) defines $\bar{\theta}_v$ in terms of other coarse-scale variables, (34) is an average over the fine-scale θ_v defined in (21)–(22), in the spirit of multiscale modeling. For instance, the coarse liquid water q_l in (34) could potentially be nonzero even if the coarse cell in bulk is unsaturated—i.e., even if $\bar{q}_t < q_{vs}(\bar{T}, \bar{p})$. In other words, MES does not require that coarse cells are either completely unsaturated or completely saturated; instead, coarse cells can be partially cloudy.

Note that the LES model does *not* use the ODT model for information about fine-scale turbulent transport; rather, the Smagorinsky scheme is retained for this purpose. Nevertheless, in principle, one could use the stochastic turbulent transport from ODT in lieu of an LES turbulent transport model such as Smagorinsky, and this should be explored in the future.

Also note that ODT would influence LES in more ways if additional physics were included. For instance, if precipitation processes were included, then additional variables and source terms would be needed for modeling droplet collision and coalescence, etc., and a multiscale coupling of these source terms would be needed. Precipitation processes will be investigated in the near future, whereas the present paper focuses on the simpler non-precipitating case.

2.4. Computational setup

The MES framework is ideal for massively parallel computations due to its "embarrassingly parallel" or "pleasantly parallel" setup. As shown in Figure 1, this is achieved by using periodic boundary conditions for each of the fine-scale line segments, which do not communicate directly with each other. This setup is different from previous hybrid models involving ODT and LES [35, 36, 37], and it is similar in spirit to the "superparameterization" approach that has been used for much larger scales of atmospheric dynamics [38, 39, 40, 41, 42]. For such a setup, one can expect excellent scalability—essentially linear—as the number of processors in increased.

Several options are explored here for ODT line configurations, as illustrated in Figure 3. The lines will be oriented along one of the three coordinate axes, and three possibilities are investigated: (i) a vertical z-line only, (ii) horizontal x- and y-lines only, and (iii) all three x-, y-, and z-lines. These choices are motivated by the anisotropic effect of gravity in atmospheric modeling. In configurations with multiple ODT lines within the same coarse cell, the lines do not interact directly; instead, they interact indirectly through the coarse-scale model. As illustrated in Figure 1, the same is true for fine-scale lines in different coarse cells, due to the periodic boundary conditions on fine scales within each coarse cell.

The time advancement algorithm for MES is as follows. Starting from coarse and fine states at coarse time T:

1. Advance the fine-scale model from T to $T + \Delta T$, using many fine-scale steps of small duration Δt, with the coarse variables held fixed. Compute the buoyancy at each coarse cell as an average over the fine scales using (34).
2. Advance the coarse-scale model from T to $T + \Delta T$, using the buoyancy averaged over the fine scales, with the fine variables held fixed.
3. Repeat.

This design is similar to previous studies [60, 61, 62], and, while it could potentially benefit from cost-saving techniques [63], little attempt has been made to further optimize efficiency for this study. In this first investigation, the focus is on simple algorithms.

The scientific setting for the simulations is shallow convection under the conditions of the field campaign called Rain In (Shallow) Cumulus over the Ocean (RICO) [64, 3]. While the field campaign was aimed at precipitating clouds, the simulations here are performed with the non-precipitating model described above. This choice is for the purpose of studying MES in a simple setting that still allows multiscale variability and interactions.

The computational grid on coarse scales is chosen as in the recent LES intercomparison study under RICO conditions [3]. The vertical grid spacing is $\Delta Z = 40$ m, and the horizontal grid spacing is $\Delta X = \Delta Y = 100$ m. Using $100 \times 128 \times 128$ coarse grid points, the domain is 4 km in height and 12.8 km in length and width. Since shallow cumulus clouds typically have length scales of $O(1)$ km, this grid provides a somewhat low resolution of a field of many clouds. Fine-scale variability in MES is modeled on line segments of length 100 m using a fine grid spacing of $\Delta x = 1$ m. The duration of all cases is 24 hours of simulated time, using a coarse-scale time step ΔT that is determined by a Courant–Friedrichs–Lewy condition. High-performance computing support was provided by NCAR's Computational and Information Systems Laboratory [65]. In addition to the MES results, LES results are also shown with the same coarse grid spacing, for comparison. All simulations in this paper are run on 128 processors, and the grid is parallelized into 16×8-column blocks that keep each vertical column intact.

The memory and computational cost of MES is intermediate between two corresponding LES cases. On the one hand, compared to coarse-resolution LES with grid spacing 100 m, MES requires greater memory by a factor of $O(100)$–$O(1000)$ due to the additional fine-scale variables. Furthermore, the computation time is greater by a factor of $O(10)$–$O(100)$ due to the fine-scale ODT dynamics. On the other hand, compared to fine-resolution LES with grid spacing 1 m—which requires $O(10^6)$ times the memory and $O(10^8)$ times the computational expense of the 100-m LES case—MES requires far less memory and far less computational expense.

3. One-way coupling

As an initial investigation of multiscale dynamics, a version of MES with one-way coupling is presented in this section. With one-way coupling, the fine-scale ODT model responds to changes in the coarse-scale LES variables, but the fine scales do *not* influence the coarse-scale dynamics. In other words, the coupling in section 2.3.1 is retained whereas the coupling in section 2.3.2 is neglected. This one-way case serves to illustrate the behavior of the LES model in stand-alone form, which is a useful baseline for comparison with the subsequent MES cases. In addition, this setup provides initial insight into the dynamics of the ODT model in response to coarse-scale convective evolution. Specifically, the question is, Does the coupling mechanism from section 2.3.1 and Figure 4 create plausible fine-scale variability?

After an initial spin-up phase, the cloud field reaches a state that is essentially in statistical equilibrium, as illustrated by the time series statistics in Figure 5. The cloud fraction is roughly 0.09, and the cloud-base and cloud-top heights are roughly 600 m and 2400 m, respectively. The vertical profile of the final state is shown in Figure 6. For each height Z, these quantities are averaged horizontally over the entire domain and over the last four hours of the simulation. The mean winds are sheared through the cloud layer; hence the clouds will hence be tilted vertically, as shown below.

With this broad view established, an individual cloud is isolated next in order to illustrate the multiscale dynamics. The cloud field is shown in Figure 7 at two vertical levels: a lower level ($Z = 800$ m) and a higher level ($Z = 1600$ m). Many clouds are visible at the lower level, whereas only a few extend vertically to $Z = 1600$ m. The dashed black lines along $Y = -1300$ m and $X = 5400$ m pass through a vigorous cloud. While the lower portion of this cloud is located near several smaller clouds (see left panel), the upper portion of the cloud is relatively isolated. The vertical structure of the cloud is shown in Figure 8 in the $Y = -1300$-m plane (top) and the $X = 5400$-m plane (bottom). In each of these panels, the vertical dashed line shows the intersection with the plane in the other panel. The cloud top is near $Z = 2000$ m, and its width is approximately 1000 m from $X = 5000$ to 6000 m. The liquid water had a maximum of roughly 1.8 g/kg near the upper central portion of the cloud. Further aspects of this particular cloud will be examined in detail in subsequent plots.

While Figures 5–8 have shown the LES evolution on coarse scales, this one-way-coupled case also includes associated fine-scale dynamics, as shown in Figure 9. Does the fine-scale variability have a plausible form? The lower-left panel of Figure 9 shows a zoomed-in view of the cloud in the $Y = -1300$-m plane, as in Figure 8. By zooming in, the liquid water in each coarse cell can be distinguished. Furthermore, 18 coarse grid cells are enclosed by a black rectangle, and the fine-scale variability within these cells are shown in the other three panels. Each coase cell has three ODT lines embedded within it: one oriented in the x direction (top left), one in the y direction (top right), and one in the z direction (bottom right). First consider the fluctuations in the ODT lines oriented in the x direction. In the top left panel, the character of the fluctuations changes from low variability in the cloud core to high variability near cloud edge. Moreover, near cloud edge, the fluctuations lead to coarse cells that are partially cloudy:

fine-scale regions of cloudy air are adjacent to clear air and are mixing together turbulently. The consequences of the cloud-clear air mixing are described further below.

In addition to differences between cloud core and cloud edge variability, Figure 9 shows different variability in ODT lines oriented in different directions. One difference is the lack of fine-scale variability on the y-oriented lines in the upper right panel of Figure 9. This is likely due to viewing a slice through the cloud in the plane $Y = -1300$ m, along which the coarse Y-derivatives are probably small. In contrast, the z-oriented lines display large fluctuations in this region where coarse Z-derivatives are large. At cloud top, one cell even has fine-scale liquid water despite being unsaturated with respect to the coarse-scale thermodynamic variables. In other words, this shows that partially cloudy air can advance into the cloud-free environment as the cloud develops. This demonstrates that the multiscale setup can produce partially cloudy cells in both scenarios: when the cell is saturated or unsaturated (with respect to the coarse-scale thermodynamic variables). In other words, this can happen on the cloudy side or the clear side of a coarse cloud edge, which consequently has a blurry definition in a multiscale model.

As a second example of the fine-scale variability, Figure 10 focuses on the lateral cloud edge away from the cloud top. While it may look like the black rectangle encloses a focus region that is near cloud base, this is not the case; as shown previously in Figure 8, the cloud is sheared in the Y direction, and the region in Figure 10 is on the lateral edge of the tilted cloud. This region includes many additional examples of coarse cells that are partially cloudy, including some cases that are unsaturated on the coarse scale (such as the $X = 5650$ m column) and some cases that are saturated on the coarse scale. Also, the y-oriented lines have significant variability in this region, since they are oriented along coarse Y-derivatives at the lateral edge of this tilted cloud.

In short, Figures 9–10 suggest that the fine-scale variability of MES is plausible. The variability is comparable to that seen in aircraft traverses through cumulus clouds (e.g., see Figure 3 of [66]). Also, the variability near cloud edges is comparable to that seen in a stand-alone model of turbulent mixing that prescribes (or "splices") initial conditions with neighboring regions of cloudy and clear air (see Figure 4 of [16]). Here, the neighboring regions of cloudy and clear air are not prescribed initially; instead, they arise through the coarse–fine coupling mechanisms, which were described in section 2.3.1 and Figure 4, and which are a natural part of the ODT algorithm.

To summarize the fine-scale variability with some basic statistics, Figure 11 shows the cloud fraction and liquid water within each coarse cell. These quantities were computed by averaging over the fine scales within each coarse cell, for each of the three embedded ODT lines. The black curve denotes the boundary of the cloud as defined by LES saturation in the coarse variables. Within the black curve are many cells that are not 100% cloudy, even though the LES variables are saturated; and outside the black curve are many cells that are partially cloudy, even though the LES variables are unsaturated. While the 100%-cloudy cells are concentrated near the cloud core, the partially cloudy cells are concentrated near cloud edges. For instance, at cloud top, one can see two partially cloudy cells that are above the LES-defined cloud boundary (in the z-oriented ODT lines in the right column of Figure 11). This partially cloudy air is advancing into the cloud-free environment as the cloud develops, and it is made possible by the multiscale coupling mechanism described in section 2.3.1.

As a final use of the one-way-coupled case, coarse LES quantities are compared directly with averages of fine-scale ODT quantities, to indicate how coarse-scale MES behavior might differ from LES behavior if two-way coupling were used for MES. For nonlinear quantities such as liquid water and buoyancy, the coarse LES definition in (5) is not necessarily the same as the average (34) over the fine-scale ODT values. The differences are shown in Figure 12 for each of the three embedded ODT lines. As in Figure 11, the black curve denotes the boundary of the cloud as defined by LES saturation in the coarse variables. Outside of this boundary, the liquid water difference cannot be negative, and it is positive for any coarse cell that is partially cloudy. Inside the cloud boundary, the ODT liquid water displays an interesting dichotomy: it is greater near the cloud top and less near the bottom of this region. The magnitude of these differences is as large as 0.1 g/kg, and the largest differences occur near cloud-top. For the virtual potential temperature θ_v, a similar pattern is seen, and the magnitude of the differences is roughly 0.1 K. The pattern in liquid water is suggestive of the effects of turbulent cloud–environment mixing: a dilution of liquid water near the top of the thermal as it advances into the cloud-free environment, and a delayed evaporation in the wake of the thermal. Furthermore, since the θ_v difference should be proportional to the buoyancy difference, the pattern in θ_v indicates how the buoyancy in two-way-coupled MES would differ from LES. In the next section, in two-way-coupled MES, it will be explored whether these differences are large enough to have a significant impact on the overall bulk cloud field properties.

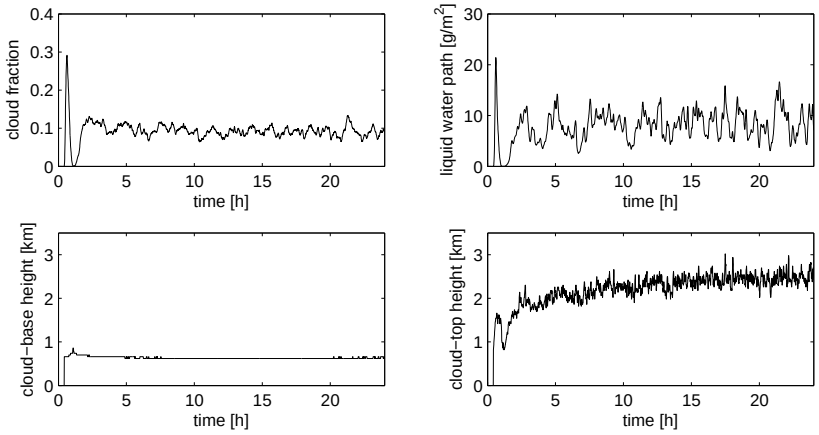

Figure 5: Time series statistics: cloud fraction (upper left), liquid water path (upper right), cloud-base height (lower left), cloud-top height (lower right).

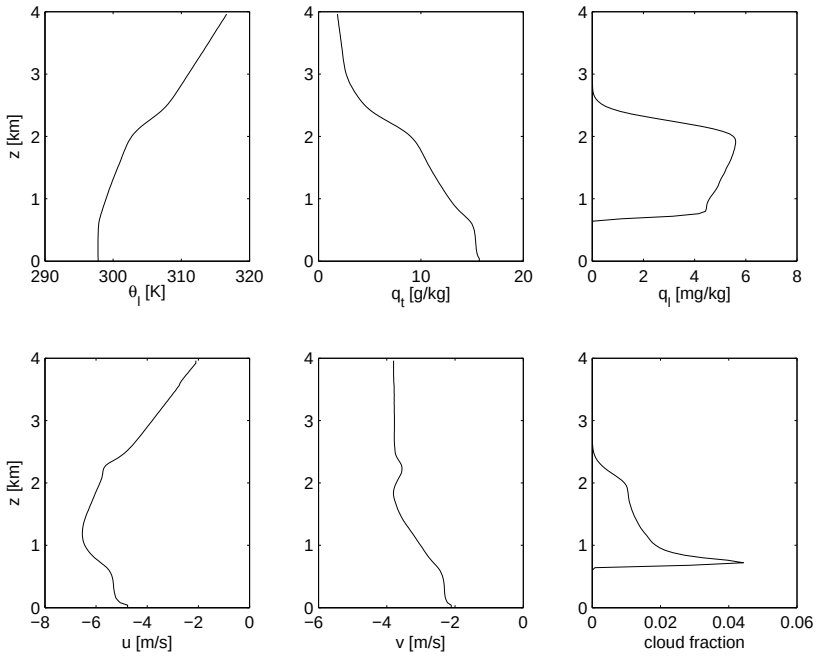

Figure 6: Profile statistics averaged horizontally and in time for the last 4 hours of the simulation at each height Z. Top row, from left to right: liquid water potential temperature θ_l, total water q_t, and liquid water q_l. Bottom row, from left to right: u, v, and cloud fraction.

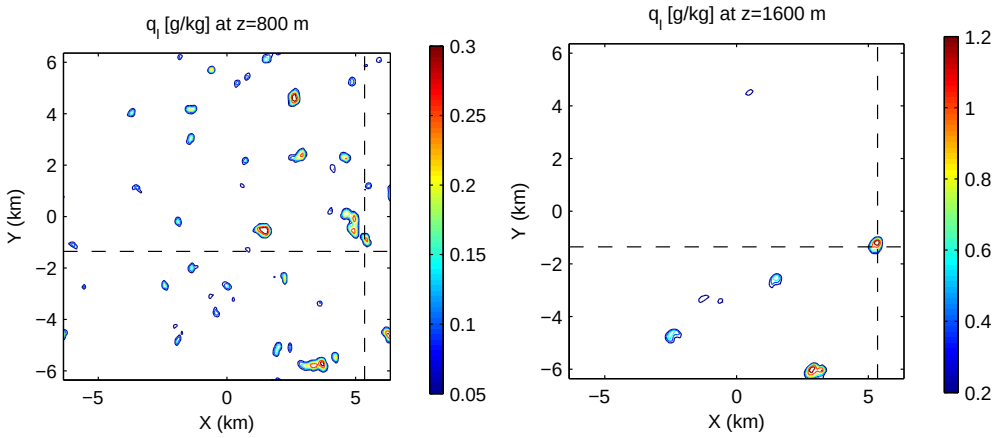

Figure 7: Liquid water at time $T = 24$ h in the $Z = 800$-m (left) and $Z = 1600$-m (right) planes. Dashed black lines are shown at $X = 5400$ m and $Y = -1300$ m, which are the locations of the slices displayed in Figure 8.

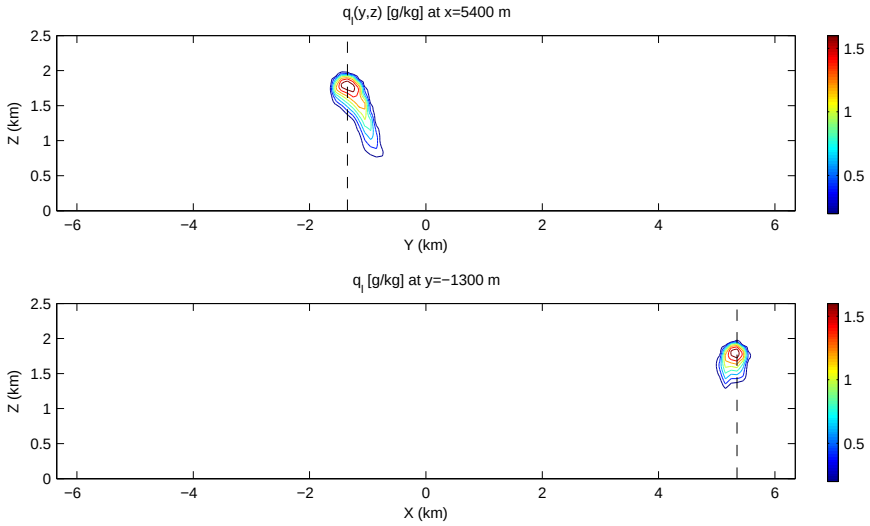

Figure 8: Liquid water at time $T = 24$ h in the $X = 5400$-m (top) and $Y = -1300$-m (bottom) planes. The dashed black line in the top plot is drawn at $Y = -1300$ m, which is the plane shown in the bottom plot; similarly, the dashed black line in the bottom plot is drawn at $X = 5400$ m, which is the plane shown in the top plot.

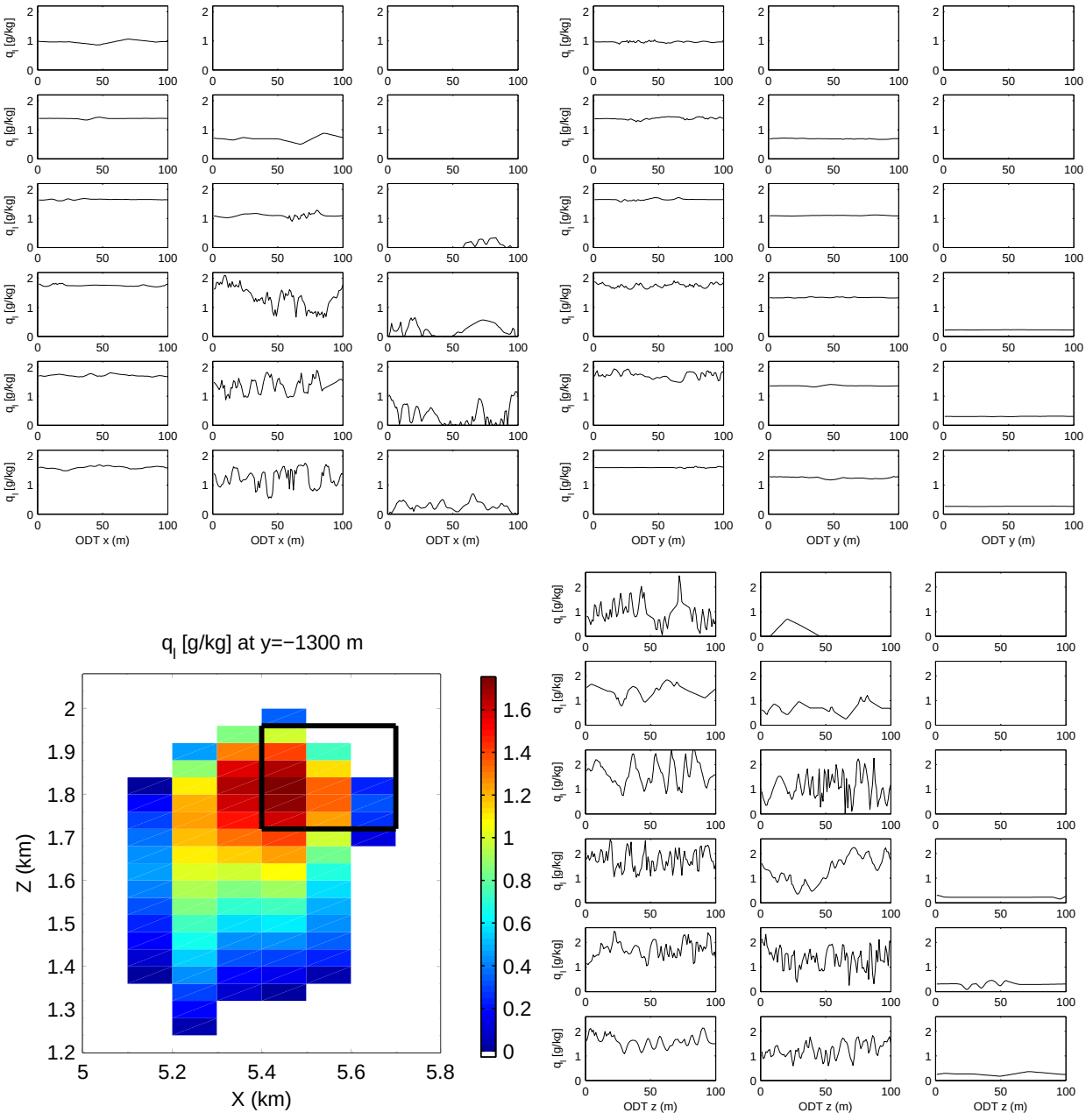

Figure 9: Liquid water on coarse scales and fine scales, at time $T = 24$ h in the $Y = -1300$-m plane. Bottom left: LES liquid water defined by the coarse-scale saturation condition and coarse-scale thermodynamic variables. The black rectangle encloses a focus region of 18 coarse grid cells near cloud top. The fine-scale liquid water in these 18 cells is shown for each of the embedded ODT lines: x-oriented lines (top right), y-oriented lines (top left), and z-oriented lines (bottom right).

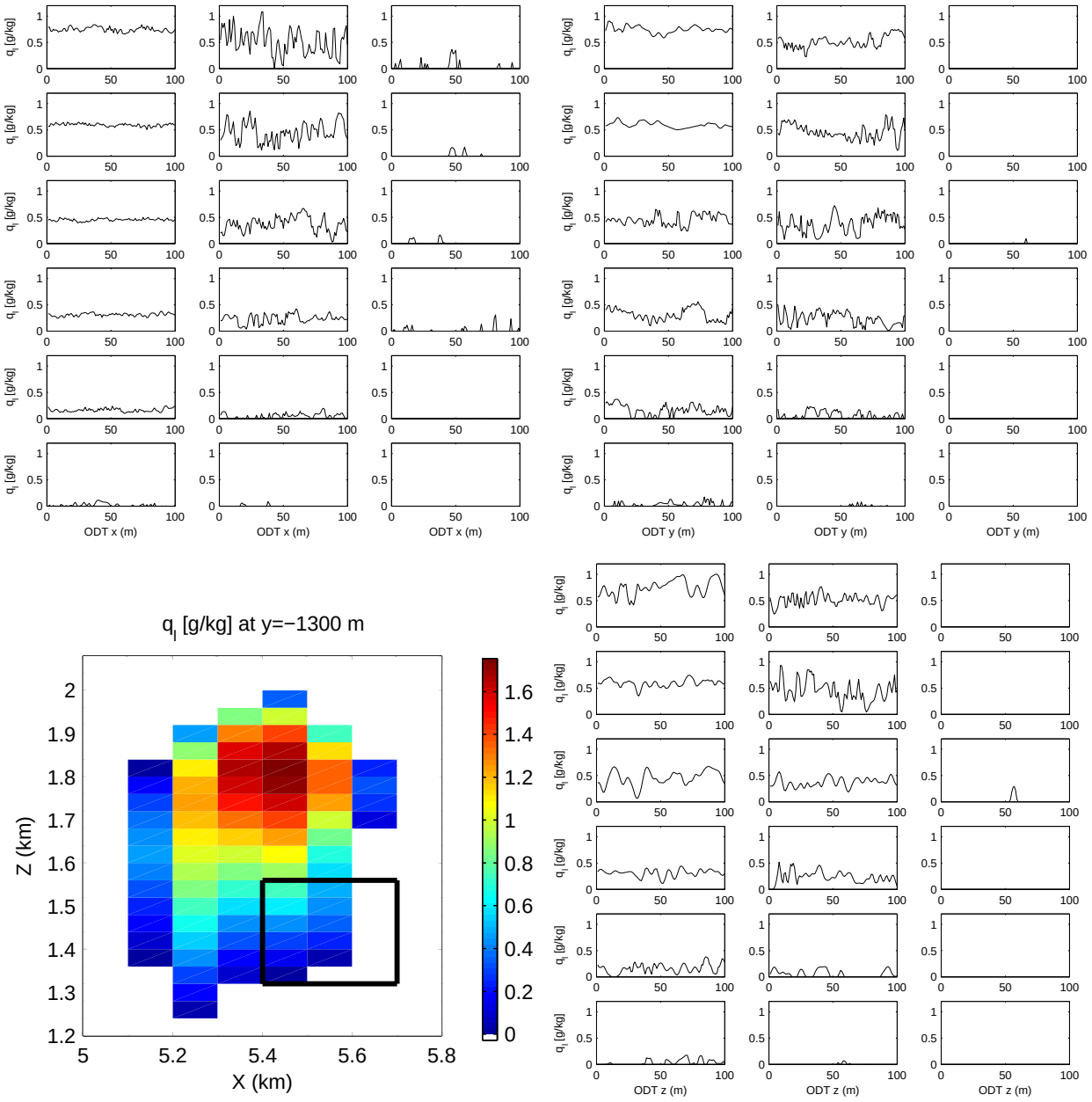

Figure 10: Liquid water on coarse scales and fine scales, at time $T = 24$ h in the $Y = -1300$-m plane. Bottom left: LES liquid water defined by the coarse-scale saturation condition and coarse-scale thermodynamic variables. The black rectangle encloses a focus region of 18 coarse grid cells on the lateral edge of this tilted cloud. The fine-scale liquid water in these 18 cells is shown for each of the embedded ODT lines: x-oriented lines (top right), y-oriented lines (top left), and z-oriented lines (bottom right).

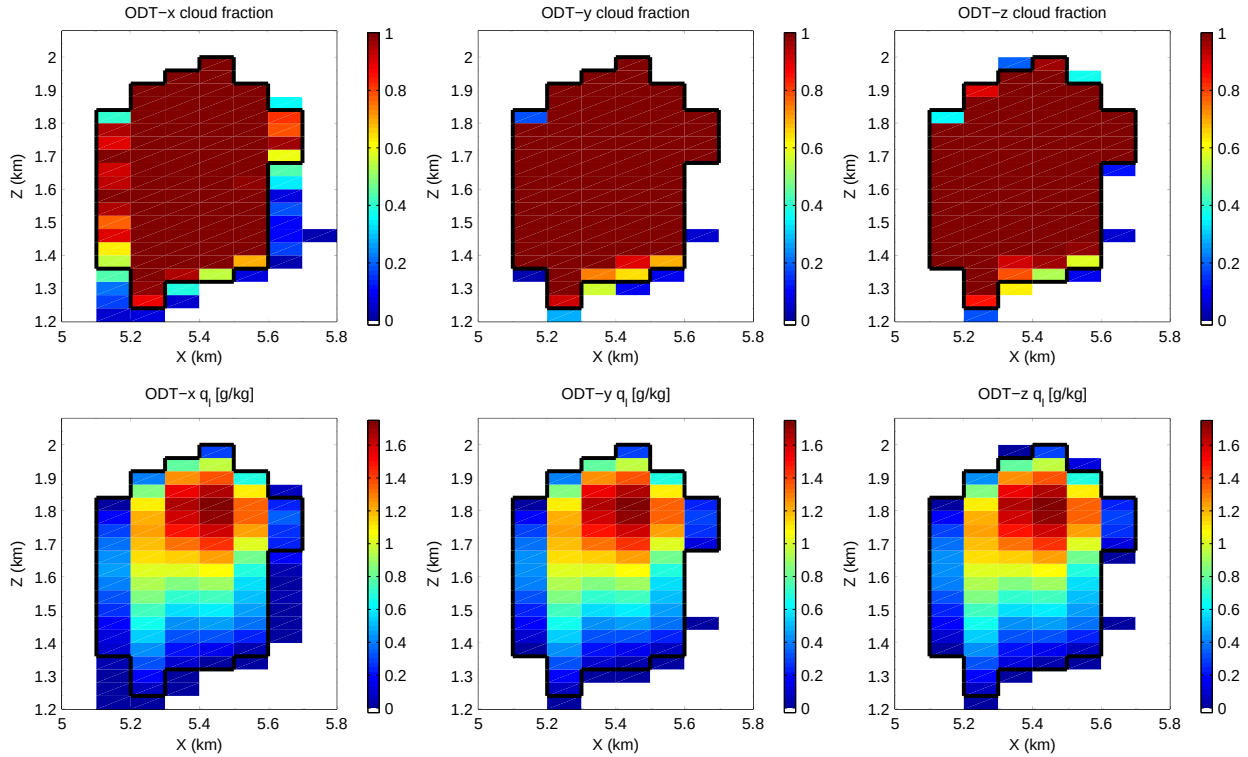

Figure 11: Cloud fraction (top) and liquid water (bottom), averaged over the fine scales within each coarse cell, for each of the three embedded ODT lines: x-oriented ODT line (left), y-oriented ODT line (middle), and z-oriented ODT line (right). The black curve denotes the boundary of the cloud as defined by LES saturation in the coarse variables.

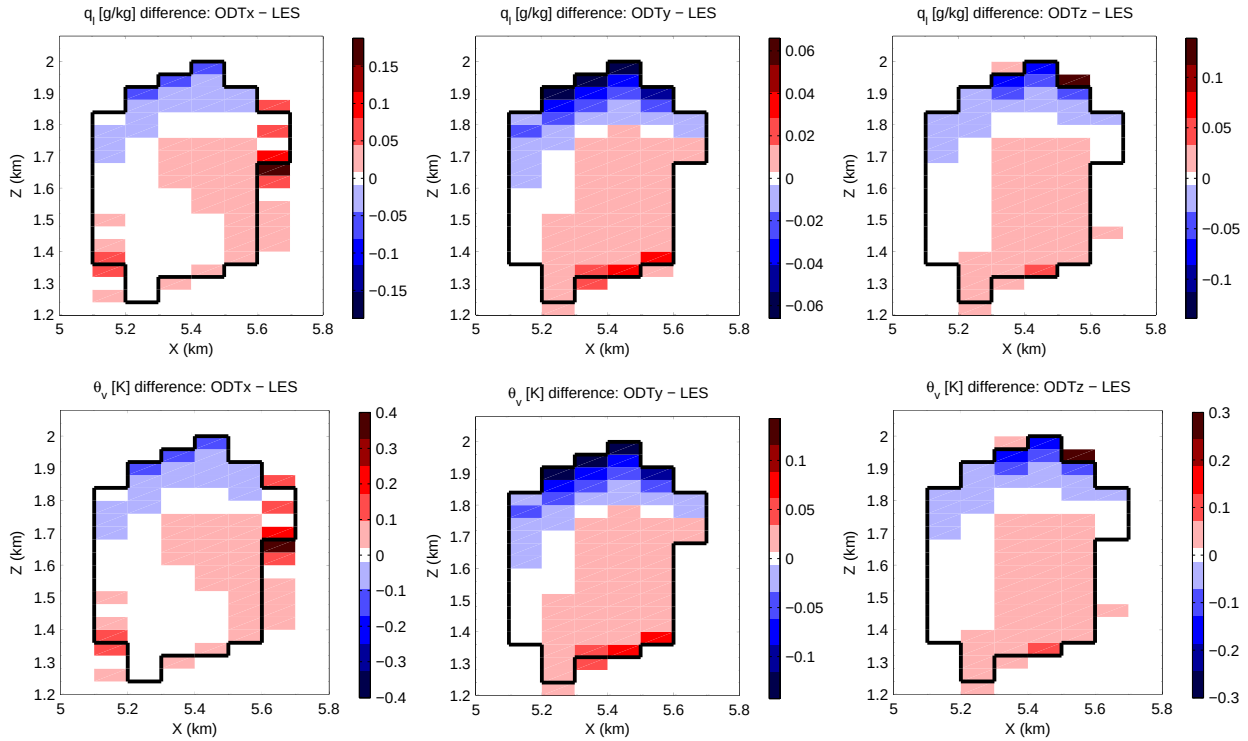

Figure 12: Differences between fine-scale-averaged quantities and coarse-scale quantities. Top: Difference in liquid water $\bar{q}_l$ defined as an average over fine-scales in (34) and as a function of coarse-scale quantities in (5). Bottom: Difference in virtual potential temperature $\bar{\theta}_v$ defined as an average over fine-scales in (34) and as a function of coarse-scale quantities in (5). Differences are computed using each of the three embedded ODT lines individually: x-oriented ODT line (left), y-oriented ODT line (middle), and z-oriented ODT line (right). The black curve denotes the boundary of the cloud as defined by LES saturation in the coarse variables.

4. Two-way coupling

In the previous section, a version of MES was investigated with one-way coupling—i.e., where the coarse LES scales influenced the fine ODT scales but not vice versa. The one-way MES was useful for comparing coarse and fine scales on a cell-by-cell basis, and it was seen that plausible fine-scale variability is produced. Here, in the present section, the full MES model is implemented with two-way coupling. Since the MES model uses a buoyancy (34) defined as an average over the fine scales, its dynamics will differ from LES. The question is then, What is the impact of the the fine-scale variability on the MES bulk cloud field properties?

Several time-series statistics were compared between LES and MES. For MES, some statistics could be defined using either the coarse-scale fluctuations or the fine-scale fluctuations or both. In what follows, unless otherwise stated, the statistics will be defined using the coarse-scale variables of MES for a first comparison of LES coarse-scale statistics versus MES coarse-scale statistics. The statistics included the ones shown in Figure 5—cloud fraction, liquid water path, cloud-base height, and cloud-top height, all of which were essentially the same for LES and MES (not shown). To probe LES and MES differences beyond three-dimensionally averaged quantities, several horizontally averaged statistics were also compared. The statistics included the ones shown in Figure 6—θ_l, q_t, q_l, u, v, and cloud fraction, all of which were essentially the same for LES and MES (not shown). This suggests that the mean coarse-scale statistics of the cloud field as a whole are similar in LES and MES. Given that plausible fine-scale variability was generated near cloud edges and cloud top, and given earlier theoretical work on the impacts of cloudy–clear-air mixing on buoyancy [14, 15, 16, 18], it was somewhat surprising to find such close similarities between MES and LES.

While the mean statistics were similar, the turbulent kinetic energy (TKE) differs between LES and MES. Figure 13 shows the time evolution of the TKE, spatially averaged in the horizontal, and integrated in the vertical direction, leaving it with units of kg/s^2. While LES and MES TKE are similar for an initial spin-up period, the LES TKE settles down into an approximate statistical equilibrium, whereas the MES TKE continues to grow slowly. Over the final 12 hours of the simulations, the average TKEs are 493 and 593 kg/s^2 for LES and MES (coarse scales), respectively. This represents a larger TKE in MES by roughly 20%. Furthermore, an extended simulation (not shown) shows that the MES TKE continues to grow slowly for at least an additional 8 hours (out to a time of $T = 32$ hours). While it is possible that this growth indicates some type of instability, further evidence suggests a simpler explanation due to ODT stochastic fluctuations. In particular, the bottom panel of Figure 13 shows that the fine-scale TKE has equilibrated, which indicates that the fine-scale fluctuations are not growing in time. Since the slow growth is seen in coarse-scale TKE but no other coarse-scale or fine-scale variable, it is likely that this growth is not due to any coherent flow structure but rather due to an accumulation of the random fluctuations introduced through the buoyancy. As was shown earlier in the bottom row of Figure 12, the fine-scale-averaged buoyancy has some rough variability from one coarse cell to another, due to the fine-scale stochastic dynamics; in the case of Figure 12, this rough variability is most pronounced in the z-oriented lines near cloud top (bottom right panel) and in the x-oriented lines near the lateral right cloud edge (bottom left panel). As further evidence of stochastic fluctuations in the buoyancy, Figure 14 shows that vertical velocity w, rather than horizontal velocity u or v, is the source of the growing TKE. In Figure 14, the horizontal spatial variance is shown, as computed at each individual vertical level, averaged over the last four hours of the simulation (from time 20 to 24 hours). While all variables have slightly larger variance in MES than LES, w clearly shows the largest difference of any of the variables. Furthermore, in an extension of the simulation for an additional 8 hours (not shown), the variance in w continues to grow, while the variance in u and v changes little. Hence it is likely that w variability is growing slowly due to stochastic variability in the buoyancy, which is defined using an average over the fine-scale stochastic variables within each coarse cell. This indicates a delicate issue in adding stochastic aspects to a fluid dynamics simulation, and this will require careful treatment when additional physical processes are added to the model in the future, such as precipitation or radiation.

While results in this section were simply labeled as "MES," they actually apply for all three of the MES configurations shown in Figure 3: one ODT line oriented in the z direction, two ODT lines oriented in the x and y directions, or three ODT lines oriented in the x, y, and z directions. The statistics described in this section are all essentially the same for each of these configurations (not shown). Nevertheless, it is possible that some detailed differences exist between the three configurations but have not yet been uncovered. This possibility is supported by the differences seen in the one-way-coupled case in Figures 9–12, which suggest some facets to investigate in the future.

Given the plausible fine-scale variability seen in the previous section, and given previous theoretical work [14,

15, 16, 18] on the impact of mixing on buoyancy, it is surprising that the fine-scale variability has little impact on the MES bulk cloud field properties. There are many possible explanations for this. As one possibility, there may be a limitation in the MES framework that is responsible. Along these lines, the Smagorinsky scheme was retained here as a closure for subgrid-scale turbulent fluxes, instead of using ODT's natural stochastic fluxes for this purpose. Also, periodic boundary conditions were used for the fine-scale model within each coarse cell, a simplification that requires justification. In other settings, this simplification has been justified a posteriori as it has led to improved models of the global atmosphere [38, 39, 40, 41, 42], improvements in ocean modeling [43], and surprising ability at simulating a squall line efficiently [67, 63]; and some test models have been developed for evaluating superparameterization algorithms [68]. Also, details of the fine-scale variability were presented here in Figures 9–12, and they suggest that the fine-scale variability is plausible, even with this use of periodic boundary conditions for the fine-scale model. Nevertheless, a detailed validation study is needed to compare MES to a moist version of high-resolution LES or to a direct numerical simulation, and results in this direction will be presented elsewhere in the future. As another possiblity, in comparing MES and earlier theoretical studies [14, 15, 16, 18], several differences are evident and might hamper a direct comparison. For instance, in the ODT-like studies of Krueger [15] and Krueger et al. [16], mixing is considered within a single parcel, an idealization that might not be directly comparable with the present paper; in MES, the 3D coarse flow evolution interacts with the ODT model and influences the sequence of eddy events. In the study of Grabowski [18], a plausible model is proposed for mixing and filamentation, yet a more detailed validation of some of the model assumptions and model parameters is still needed. Moreover, the model of Grabowski [18] is meant to represent mixing and subsequent *microscale* homogenization, which is perhaps not fully represented here with an ODT grid spacing of 1 m. In any case, while evidence was presented here to suggest that the MES fine-scale variability is plausible, a quantitative validation study is needed and will be presented elsewhere in the future.

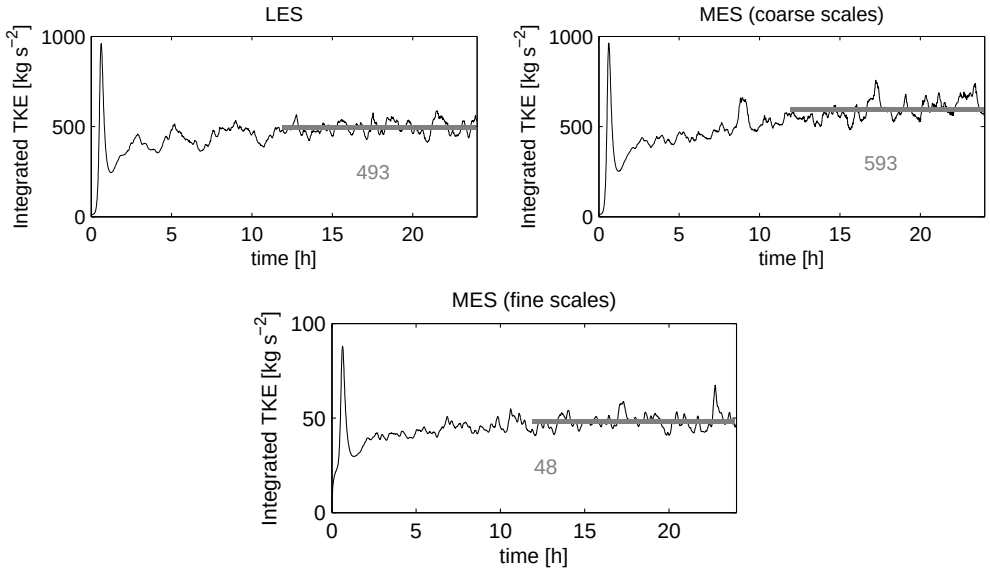

Figure 13: Time evolution of turbulent kinetic energy, integrated over the entire three-dimensional domain, for cases of LES (upper left) and MES, with MES coarse-scale TKE (upper right) shown separately from MES fine-scale TKE (bottom). The horizontal gray lines indicate the average values over the last 12 hours of the simulations: 493 kg/s^2 for LES (upper left), 593 kg/s^2 for MES coarse scales (upper right), and 48 kg/s^2 for MES fine scales (bottom). Notice the different axis range in the bottom panel.

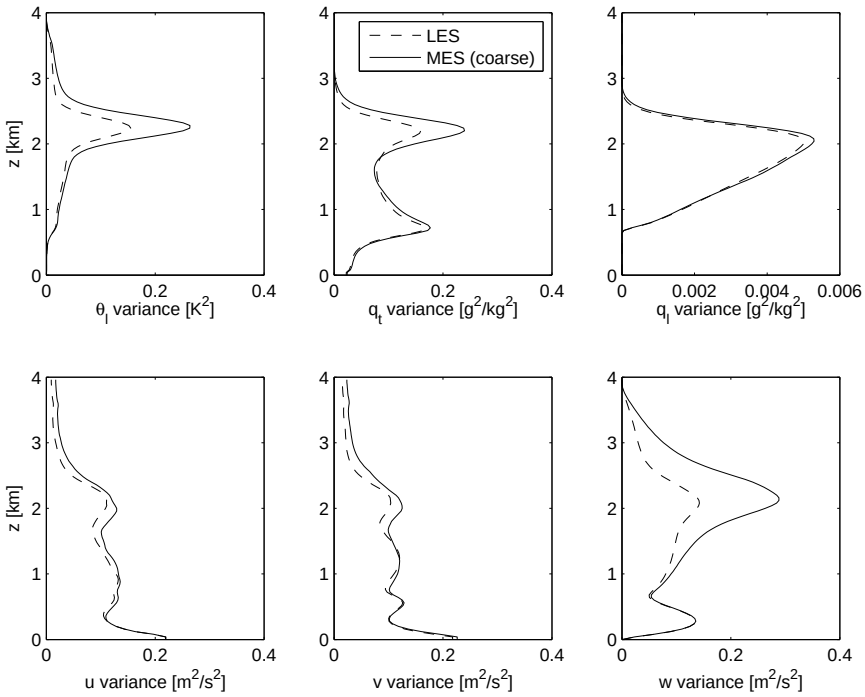

Figure 14: Horizontal spatial variances, at each vertical level, averaged over the last four hours of the simulation. Top row, from left to right: liquid water potential temperature θ_l, total water q_t, and liquid water q_l. Bottom row, from left to right: velocity components u, v, and w. LES is denoted by dashed lines, and MES (coarse scales) is denoted by solid lines.

5. Concluding discussion

A multiscale framework was designed and investigated for modeling convection and cloud dynamics. Motivated by limitations of traditional LES, a key goal is to include more realistic behavior on fine scales, such as turbulent mixing between cloudy and clear air. Called "multiscale eddy simulation" (MES), the framework uses LES to represent the coarse scales of >100 m and a stochastic, one-dimensional turbulence model to represent the fine scales of < 100 m. The coupling between coarse and fine scales is designed to be "embarrassingly parallel" or "pleasantly parallel"—and hence ideal for massively parallel computations. In this first investigation, to provide evidence of the plausibility of the fine-scale dynamics, the coarse–fine coupling mechanism is described in detail, and the fine-scale variability is illustrated; but a quantitative validation study is left as an important next step for future work. Furthermore, the focus of this first investigation is on the buoyancy and on the fine-scale mixing process (of cloudy and clear air) that can affect the buoyancy. To isolate this effect alone, the ODT model does not supply the coarse-scale LES model with its stochastic turbulent fluxes, and the Smagorinsky closure is retained for this purpose as a model for the fine-scale turbulent fluxes.

The multiscale dynamics was illustrated in simulations of a shallow cumulus cloud field. In a simulation with one-way coupling, where the fine scales did not influence the coarse scales, the fine-scale variability was shown in detail and was seen to take a plausible form. Partially cloudy grid cells were seen to be prominent, particularly near cloud edges and cloud top. From earlier theoretical work [14, 15, 16, 18], this mixing of cloudy and clear air is believed to have an important impact on buoyancy; and, in a cell-by-cell comparison, MES and LES buoyancy were seen to differ. In simulations with full two-way coupling, however, contrary to expectations based on earlier theoretical studies, the mean statistics of the bulk cloud field are essentially the same in MES and LES. Possible reasons for this were discussed in section 4. For instance, it is possible that some aspects of the earlier theoretical work are not carried over to the cases considered here. It is also possible that there are limitations in the present formulation of MES, such as the absence of any explicit "splicing" [58, 15, 16], although the discussion in section 2.3.1 suggested that a similar effect is included naturally in the ODT algorithm. In any case, it is likely that MES and LES properties will diverge further as more nonlinear physical processes—such as precipitation—are included, and results in this direction will be presented elsewhere in the future.

One aspect that requires attention in the future is the appropriate filtering of stochastic sources in the fluid flow model. For the MES cases shown here, the coarse-scale TKE showed a slow growth in time. This is in contrast to the fine-scale TKE and all mean statistics of the bulk cloud field, which all reach a statistical equilibrium. The most likely cause of the slow growth is stochastic fluctuations in the buoyancy, which perhaps require some spatial and/or temporal filtering to attenuate stochastic roughness. A similar issue was readily apparent in our initial explorations (not shown) into using ODT turbulent fluxes in place of the Smagorinsky closure (which could be formulated following section III.E. of [59]). The ODT turbulent fluxes showed a very high degree of stochastic variability, some of which is a representation of actual variability in the fine-scale turbulent fluxes, and some of which is due to statistical undersampling. For the future, a way of imporoving the sampling will be needed, perhaps either through some type of filter or through the addition of more ODT lines.

Further studies are needed to better validate MES. While the ODT model has been validated in stand-alone form, a new validation should be carried out for each new application. For the simulations presented here, ODT was used only to provide the buoyancy for the coarse-scale model, and it was suggested that MES represents the important cloud processes that determine buoyancy (in particular, a representation of entrainment events and subsequent mixing of cloudy and clear air). In the future, as we explore the use of the ODT model in an expanded role in place of a traditional LES closure for turbulent fluxes, more detailed validation studies will be crucial to quantify the realism of the modeled turbulent transport. For the case of interest here, it would be appropriate to compare MES to a moist version of high-resolution LES or to a direct numerical simulation, and results in this direction will be presented elsewhere in the future.

Returning to the overarching scientific motivation, MES provides a promising approach for understanding aerosol–cloud–precipitation–climate relationships. At the heart of these issues are complex interactions, across a vast range of scales, of turbulent fluid dynamics and liquid droplets [11, 12, 21, 69, 70]. By representing dynamics for a wider range of these scales, it is hoped that MES will help bridge gaps in our understanding of these multiscale processes.

Acknowledgments

The research of S. N. S. is partially supported by grant NSF DMS–1209409. S. N. S. extends his thanks to B. Stevens for helpful discussion, guidance, and support for this research; to Rupert Klein and an anonymous reviewer for comments that significantly improved the presentation in many ways; to A. Majda for initially bringing the ODT model to his attention; to the Max-Planck-Institut für Meteorologie, where a portion of this work was carried out, for providing visitor travel funds and accomodation; to A. Kerstein and S. Krueger for helpful discussion; and to A. Kerstein and S. Wunsch for providing ODT source code.

References

[1] M. Khairoutdinov, D. Randall, High-resolution simulation of shallow-to-deep convection transition over land, J. Atmos. Sci. 63 (2006) 3421–3436.
[2] G. Matheou, D. Chung, L. Nuijens, B. Stevens, J. Teixeira, On the fidelity of large-eddy simulation of shallow precipitating cumulus convection, Mon. Wea. Rev. 139 (2011) 2918–2939.
[3] M. C. van Zanten, Margreet, B. Stevens, L. Nuijens, A. P. Siebesma, A. S. Ackerman, F. Burnet, A. Cheng, F. Couvreux, H. Jiang, M. Khairoutdinov, et al., Controls on precipitation and cloudiness in simulations of trade-wind cumulus as observed during RICO, J. Adv. Model. Earth Syst. 3 (2011) M06001.
[4] R. Houze, Cloud dynamics, Academic Press, San Diego, 1993.
[5] K. A. Emanuel, Atmospheric Convection, Oxford University Press, 1994.
[6] H. R. Pruppacher, J. D. Klett, Microphysics of clouds and precipitation, Kluwer Academic Publishers, Dordrecht, 1997.
[7] G. Sommeria, J. W. Deardorff, Subgrid-scale condensation in models of nonprecipitating clouds, J. Atmos. Sci. 34 (1977) 344–355.
[8] B. Stevens, R. L. Walko, W. R. Cotton, G. Feingold, The spurious production of cloud-edge supersaturations by Eulerian models, Mon. Wea. Rev. 124 (1996) 1034–1041.
[9] L. Margolin, J. M. Reisner, P. K. Smolarkiewicz, Application of the volume-of-fluid method to the advection–condensation problem, Mon. Wea. Rev. 125 (1997) 2265–2273.
[10] C. A. Jeffery, J. M. Reisner, A study of cloud mixing and evolution using PDF methods. Part I: Cloud front propagation and evaporation, J. Atmos. Sci. 63 (2006) 2848–2864.
[11] M. B. Pinsky, A. P. Khain, Turbulence effects on droplet growth and size distribution in clouds–A review, J. Aerosol Sci. 28 (1997) 1177–1214.
[12] R. Shaw, Particle–turbulence interactions in atmospheric clouds, Annu. Rev. Fluid Mech. 35 (2003) 183–227.
[13] W. W. Grabowski, L.-P. Wang, Growth of cloud droplets in a turbulent environment, Annu. Rev. Fluid Mech. 45 (2013) 293–324.
[14] W. W. Grabowski, Cumulus entrainment, fine-scale mixing, and buoyancy reversal, Q. J. Royal Meteor. Soc. 119 (1993) 935–956.
[15] S. Krueger, Linear eddy modeling of entrainment and mixing in stratus clouds, J. Atmos. Sci. 50 (1993) 3078–3090.
[16] S. Krueger, C. Su, P. McMurtry, Modeling entrainment and finescale mixing in cumulus clouds, J. Atmos. Sci. 54 (1997) 2697–2712.
[17] C. Su, S. Krueger, P. McMurtry, P. Austin, Linear eddy modeling of droplet spectral evolution during entrainment and mixing in cumulus clouds, Atmos. Res. 47 (1998) 41–58.
[18] W. W. Grabowski, Representation of turbulent mixing and buoyancy reversal in bulk cloud models, J. Atmos. Sci. 64 (2007) 3666–3680.
[19] H. Morrison, W. W. Grabowski, Modeling supersaturation and subgrid-scale mixing with two-moment bulk warm microphysics, J. Atmos. Sci. 65 (2008) 792–812.
[20] A. Seifert, L. Nuijens, B. Stevens, Turbulence effects on warm-rain autoconversion in precipitating shallow convection, Quart. J. Roy. Meteor. Soc. 136 (2010) 1753–1762.
[21] E. Bodenschatz, S. P. Malinowski, R. A. Shaw, F. Stratmann, Can we understand clouds without turbulence?, Science 327 (2010) 970.
[22] B. Stevens, G. Feingold, Untangling aerosol effects on clouds and precipitation in a buffered system, Nature 461 (2009) 607–613.
[23] A. R. Kerstein, One-dimensional turbulence: model formulation and application to homogeneous turbulence, shear flows, and buoyant stratified flows, J. Fluid Mech. 392 (1999) 277–334.
[24] A. R. Kerstein, W. T. Ashurst, S. Wunsch, V. Nilsen, One-dimensional turbulence: vector formulation and application to free shear flows, J. Fluid Mech. 447 (2001) 85–109.
[25] S. Wunsch, A. R. Kerstein, A stochastic model for high-Rayleigh-number convection, J. Fluid Mech. 528 (2005) 173–205.
[26] A. R. Kerstein, S. Wunsch, Simulation of a stably stratified atmospheric boundary layer using one-dimensional turbulence, Boundary-Layer Meteorology 118 (2006) 325–356.
[27] H. Schmidt, A. R. Kerstein, S. Wunsch, R. Nédélec, B. J. Sayler, Analysis and numerical simulation of a laboratory analog of radiatively induced cloud-top entrainment, Theor. Comp. Fluid Dyn. 27 (2013) 377–395.
[28] J. E. Broadwell, R. E. Breidenthal, A simple model of mixing and chemical reaction in a turbulent shear layer, J. Fluid Mech. 125 (1982) 397–410.
[29] M. Baker, R. Breidenthal, T. Choularton, J. Latham, The effects of turbulent mixing in clouds, J. Atmos. Sci. 41 (1984) 299–304.
[30] J. B. Jensen, M. B. Baker, A simple model of droplet spectral evolution during turbulent mixing, J. Atmos. Sci. 46 (1989) 2812–2829.
[31] A. R. Kerstein, Linear-eddy modelling of turbulent transport. Part 6. Microstructure of diffusive scalar mixing fields, J. Fluid Mech. 231 (1991) 361–394.
[32] N. Peters, Turbulent Combustion, Cambridge Univ Press, Cambridge, 2000.
[33] T. Echekki, A. R. Kerstein, T. D. Dreeben, J. Y. Chen, 'One-dimensional turbulence' simulation of turbulent jet diffusion flames: model formulation and illustrative applications, Combustion and Flame 125 (2001) 1083–1105.
[34] A. J. Ricks, J. C. Hewson, A. R. Kerstein, J. P. Gore, S. R. Tieszen, W. T. Ashurst, A spatially developing one-dimensional turbulence (ODT) study of soot and enthalpy evolution in meter-scale buoyant turbulent flames, Combustion Science and Technology 182 (2010) 60–101.

[35] S. Cao, T. Echekki, A low-dimensional stochastic closure model for combustion large-eddy simulation, J. Turbulence 9 (2008) N2.
[36] R. Schmidt, A. Kerstein, R. McDermott, ODTLES: A multi-scale model for 3D turbulent flow based on one-dimensional turbulence modeling, Comput. Methods Appl. Mech. Engrg. 199 (2010) 865–880.
[37] E. D. Gonzalez-Juez, R. C. Schmidt, A. R. Kerstein, ODTLES simulations of wall-bounded flows, Physics of Fluids 23 (2011) 125102.
[38] W. W. Grabowski, P. K. Smolarkiewicz, CRCP: a Cloud Resolving Convection Parameterization for modeling the tropical convecting atmosphere, Physica D: Nonlinear Phenomena 133 (1999) 171–178.
[39] W. W. Grabowski, Coupling cloud processes with the large-scale dynamics using the cloud-resolving convection parameterization (CRCP)., J. Atmos. Sci. 58 (2001) 978–997.
[40] M. F. Khairoutdinov, D. A. Randall, A cloud resolving model as a cloud parameterization in the NCAR Community Climate System Model: Preliminary results, Geophys. Res. Lett. 28 (2001) 3617–3620.
[41] D. Randall, M. Khairoutdinov, A. Arakawa, W. Grabowski, Breaking the cloud parameterization deadlock, Bull. Amer. Meteor. Soc. 84 (2003) 1547–1564.
[42] M. Khairoutdinov, D. Randall, C. Demott, Simulations of the atmospheric general circulation using a cloud-resolving model as a superparameterization of physical processes., Journal of Atmospheric Sciences 62 (2005) 2136–2154.
[43] J.-M. Campin, C. Hill, H. Jones, J. Marshall, Super-parameterization in ocean modeling: Application to deep convection, Ocean Modelling 36 (2011) 90–101.
[44] I. Grooms, A. J. Majda, Efficient stochastic superparameterization for geophysical turbulence, Proc. Natl. Acad. Sci. USA 110 (2013) 4464–4469.
[45] J.-H. Liang, J. C. McWilliams, P. P. Sullivan, B. Baschek, Modeling bubbles and dissolved gases in the ocean, J. Geophys. Res 116 (2011) C03015.
[46] R. Klein, Scale-dependent models for atmospheric flows, Annu. Rev. Fluid Mech. 42 (2010) 249–274.
[47] B. Khouider, A. J. Majda, S. N. Stechmann, Climate science in the tropics: waves, vortices and PDEs, Nonlinearity 26 (2013) R1–R68.
[48] A. Z. Owinoh, B. Stevens, R. Klein, Multiscale asymptotics analysis for the mesoscale dynamics of cloud-topped boundary layers, J. Atmos. Sci. 68 (2011) 379–402.
[49] S. N. Stechmann, B. Stevens, Multiscale models for cumulus cloud dynamics, J. Atmos. Sci. 67 (2010) 3269–3285.
[50] B. Stevens, Atmospheric moist convection, Annu. Rev. Earth Planet. Sci. 33 (2005) 605–643.
[51] S. Bony, J. Dufresne, Marine boundary layer clouds at the heart of tropical cloud feedback uncertainties in climate models, Geophys. Res. Lett 32 (2005) 20806.
[52] J. Heintzenberg, R. J. Charlson (Eds.), Clouds in the Perturbed Climate System, The MIT Press, Cambridge, 2009.
[53] B. A. Albrecht, Aerosols, cloud microphysics, and fractional cloudiness, Science 245 (1989) 1227–1230.
[54] Z. Levin, W. R. Cotton (Eds.), Aerosol pollution impact on precipitation: A scientific review, Springer, 2008.
[55] D. Rosenfeld, U. Lohmann, G. B. Raga, C. D. O'Dowd, M. Kulmala, S. Fuzzi, A. Reissell, M. O. Andreae, Flood or drought: How do aerosols affect precipitation?, Science 321 (2008) 1309–1313.
[56] B. Stevens, A. Seifert, Understanding macrophysical outcomes of microphysical choices in simulations of shallow cumulus convection, J. Meteor. Soc. Japan 86A (2008) 143–162.
[57] B. Stevens, C.-H. Moeng, A. S. Ackerman, C. S. Bretherton, A. Chlond, S. de Roode, J. Edwards, J.-C. Golaz, H. Jiang, M. Khairoutdinov, et al., Evaluation of large-eddy simulations via observations of nocturnal marine stratocumulus, Mon. Wea. Rev. 133 (2005) 1443–1462.
[58] P. A. McMurtry, S. Menon, A. R. Kerstein, A linear eddy sub-grid model for turbulent reacting flows: Application to hydrogen-air combustion, Symposium (International) on Combustion 24 (1992) 271–278.
[59] E. D. Gonzalez-Juez, A. R. Kerstein, L. H. Shih, Vertical mixing in homogeneous sheared stratified turbulence: A one-dimensional-turbulence study, Physics of Fluids 23 (2011) 055106.
[60] W. W. Grabowski, An improved framework for superparameterization., J. Atmos. Sci. 61 (2004) 1940–1952.
[61] A. J. Majda, S. N. Stechmann, A simple dynamical model with features of convective momentum transport, J. Atmos. Sci. 66 (2009) 373–392.
[62] S. N. Stechmann, A. J. Majda, D. Skjorshammer, Convectively coupled wave–environment interactions, Theor. Comp. Fluid Dyn. 27 (2013) 513–532.
[63] Y. Xing, A. J. Majda, W. W. Grabowski, New efficient sparse space-time algorithms for superparameterization on mesoscales, Monthly Weather Review 137 (2009) 4307–4324.
[64] R. M. Rauber, B. Stevens, H. T. Ochs, C. Knight, B. A. Albrecht, A. M. Blyth, C. W. Fairall, J. B. Jensen, S. G. Lasher-Trapp, O. L. Mayol-Bracero, et al., Rain in shallow cumulus over the ocean: The RICO campaign, Bull. Amer. Meteor. Soc. 88 (2007) 1912–1928.
[65] Computational and Information Systems Laboratory. 2013. Yellowstone: IBM iDataPlex System (University Community Computing). Boulder, CO: National Center for Atmospheric Research. http://n2t.net/ark:/85065/d7wd3xhc, 2013.
[66] J. Warner, The water content of cumuliform cloud, Tellus 7 (1955) 449–457.
[67] W. W. Grabowski, Comments on "Preliminary tests of multiscale modeling with a two-dimensional framework: sensitivity to coupling methods", Mon. Wea. Rev. 134 (2006) 2021–2026.
[68] A. J. Majda, M. J. Grote, Mathematical test models for superparametrization in anisotropic turbulence, Proc. Natl. Acad. Sci. 106 (2009) 5470–5474.
[69] S. Gerashchenko, G. Good, Z. Warhaft, Entrainment and mixing of water droplets across a shearless turbulent interface with and without gravitational effects, J. Fluid Mech. 668 (2011) 293–303.
[70] G. H. Good, S. Gerashchenko, Z. Warhaft, Intermittency and inertial particle entrainment at a turbulent interface: the effect of the large-scale eddies, J. Fluid Mech. 694 (2012) 371–398.